AGU ADVANCING EARTH AND SPACE SCIENCE

Geophysical Research Letters

RESEARCH LETTER
10.1029/2020GL089476

Exploring the ENSO Impact on Basin-Scale Floods Using Hydrological Simulations and TRMM Precipitation

Yan Yan[1,2], Huan Wu[1,3,4], Guojun Gu[4], Philip J. Ward[5], Lifeng Luo[6], Xiaomeng Li[1,3], Zhijun Huang[1,3], and Jing Tao[7,8]

[1]School of Atmospheric Sciences, Sun Yat-sen University, and Key Laboratory of Tropical Atmosphere-Ocean System, Ministry of Education, and Southern Marine Science and Engineering Guangdong Laboratory (Zhuhai), Zhuhai, China, [2]Department of Atmospheric and Oceanic Sciences and Institute of Atmospheric Sciences, Fudan University, Shanghai, China, [3]Guangdong Province Key Laboratory for Climate Change and Natural Disaster Studies, Sun Yat-sen University, Zhuhai, China, [4]Earth System Science Interdisciplinary Center, University of Maryland, College Park, MD, USA, [5]Institute for Environmental Studies, Vrije Universiteit Amsterdam, Amsterdam, The Netherlands, [6]Department of Geography, Environment, and Spatial Sciences, Michigan State University, East Lansing, MI, USA, [7]Climate and Ecosystem Sciences Division, Lawrence Berkeley National Laboratory, Berkeley, CA, USA, [8]Civil and Environmental Engineering University of Washington, Seattle, WA, USA

Key Points:
- Simultaneous correlations between flood indices and Nino 3.4 appear in many flood-prone river basins in the tropics and midlatitudes
- ENSO-leading-floods relations gauged by significant lag-correlations between floods and Nino 3.4 can also be seen in many river basins
- These ENSO-floods-relations can greatly help our efforts of exploring basin-scale monthly-to-seasonal flood predictability

Supporting Information:
- Supporting Information S1

Correspondence to:
H. Wu,
wuhuan3@mail.sysu.edu.cn

Citation:
Yan, Y., Wu, H., Gu, G., Ward, P. J., Luo, L., Li, X., et al. (2020). Exploring the ENSO impact on Basin-scale floods using hydrological simulations and TRMM precipitation. *Geophysical Research Letters*, *47*, e2020GL089476. https://doi.org/10.1029/2020GL089476

Received 13 JUL 2020
Accepted 5 NOV 2020
Accepted article online 9 NOV 2020

Abstract El Niño-Southern Oscillation (ENSO) is an important driver of interannual climate variability with increasing attention for its impacts on water and flood management. The impact of ENSO on basin-scale floods during the TRMM period (1998–2013) is examined by using the streamflow outputs from the Dominant river Routing Integrated with VIC Environment model (DRIVE). Significant simultaneous correlations between flood indices and Niño 3.4 appear in many flood-prone river basins during peak flood months across both the tropics and midlatitudes especially for flood frequency and flood duration. Gauged by significant lag-correlations between floods and Niño 3.4, significant ENSO-leading-floods relations are found as well in many river basins in South America, south and southeastern Asia, and northern Africa. These ENSO-floods-relations can greatly enhance understanding of physical mechanisms relevant to the ENSO impact and may also improve the skills of basin-scale monthly-to-seasonal flood forecast, thus allowing for better preparedness and management of flood risks.

Plain Language Summary As a naturally occurring phenomenon involving quasi-periodic variation of air pressure and sea surface temperature, the ENSO impacts global floods through its modulation of atmospheric circulations, weather, and precipitation. Previous studies on ENSO-floods-relations are often limited in supporting practical flood disaster preparedness and risk analyses because of the lack of a "complete" reconstruction of past flood events likely due to scattered gauge-based streamflow data and/or coarse-resolution retrospective simulations. Here flood events at model grids and for individual river basins are identified using the outputs from the Dominant river Routing Integrated with VIC Environment model (DRIVE) with a high spatial resolution (0.125° × 0.125°) driven by the state-of-the-art satellite precipitation product TMPA. Simultaneous and lagged responses of basin-scale floods to ENSO are explored to provide an improved knowledge of the ENSO effect on global floods and a guidance for flood disaster planning and risk management for the regions consistently impacted by ENSO.

1. Introduction

The El Niño-Southern Oscillation (ENSO) is a dominant physical mode on the interannual time scale within the coupled atmosphere-ocean system (e.g., Kumar & Hoerling, 2003; Trenberth et al., 1998). It can significantly modulate precipitation patterns in the tropics by affecting large-scale circulation systems and also cause climate anomalies and precipitation variations in the mid-high latitudes of both hemispheres through distinct teleconnection mechanisms (e.g., Curtis & Adler, 2003; Dai & Wigley, 2000; Ropelewski & Halpert, 1987). Consequently, ENSO can impact global floods (e.g., Chiew & McMahon, 2002; Emerton et al., 2017; Lee et al., 2018a, 2018b; Ward, Eisner, et al., 2014; Ward, Jongman, et al., 2014; Ward et al., 2016), given the intrinsic connections between precipitation and the occurrence of flood events. Precipitation has thus even been applied as a direct predictor for floods (e.g., Stephens et al., 2015), even though the

occurrence of floods also depends on antecedent surface conditions and other factors (e.g., Berghuijs et al., 2016; Emerton et al., 2017, 2018, 2019; Sharma et al., 2018).

The connection between ENSO and flood variation has been explored in previous studies using in situ gauge observations (e.g., Andrews et al., 2004; Archfield et al., 2016; Dettinger & Diaz, 2000; Ward et al., 2010). For instance, using monthly streamflow data from 1,345 gauges, Dettinger and Diaz (2000) showed that significant correlations between ENSO and streamflows could be found in various river basins over global continents. By means of the Global Runoff Database, Ward et al. (2010) discovered that ENSO tends to have a more intense effect on annual high-flow events than on mean annual discharges, particularly in the extratropics.

Because of limited spatial coverage and temporal inhomogeneity of in situ streamflow observations, hydrological simulations have become an important complement and perhaps a critical tool for exploring variations and changes of global floods on the interannual-to-interdecadal time scales, including examining the relationships between ENSO and floods (e.g., Emerton et al., 2017; Lee et al., 2018a, 2018b; Ward, Eisner, et al., 2014; Ward et al., 2016; Yan et al., 2020). A short summary of observations and modeling information applied for the ENSO-flood relations in past studies is provided in the supporting information Table S1. These retrospective simulations can generally provide a reasonable account of global floods, which cannot be derived solely from in situ gauge observations. However, past studies performed simulations of streamflows and floods often at a relatively coarse spatial resolution (e.g., Emerton et al., 2017; Ward, Eisner, et al., 2014; Ward et al., 2016). Using the streamflow retrospective simulations from the Dominant river Routing Integrated with VIC Environment model (DRIVE) driven by the high-quality, high spatiotemporal resolution satellite-based precipitation estimates from the NASA/TRMM Multisatellite Precipitation Analysis (TMPA; Huffman et al., 2007), Yan et al. (2020) provided a detailed account of climatological and seasonal mean features of floods during the TRMM era (1998–2013). They primarily concentrated on floods and precipitation at the resolution of model grids and were generally focused on the simultaneous correlation relations between ENSO and floods. Here we advance further by focusing on floods at the basin scale. Specifically, we intend to explore the connections between ENSO and basin-scale floods and compare this with the ENSO impact on basin-scale precipitation. This can provide a "collective" measure of the ENSO impact on individual river basins. The simultaneous and lagged correlations relations between ENSO and floods on the basin scale are quantified. The possible lag-relations between ENSO and floods can improve flood forecasts and/or flood impact forecasts (Nobre et al., 2019). The simultaneous and lagged connections between precipitation over individual river basins and ENSO are also explored, though the ENSO effects on precipitation and river flows/floods might be different for many river basins (e.g., Emerton et al., 2017). Therefore, the primary objective of this study is to provide an improved understanding of the ENSO effect on basin-scale flood events. An improved understanding of simultaneous and lagged responses of basin-scale river flows/floods to ENSO, in addition to the connections between precipitation and ENSO, could greatly help our efforts of exploring monthly/seasonal flood predictability (e.g., Chiew & McMahon, 2002; Lee et al., 2018a), thus allowing for better preparedness and management of flood risks, such as more appropriately preallocating and prioritizing mitigation resources (Wu et al., 2020).

2. Data and Methodology

The DRIVE retrospective simulations were performed using the TRMM/TMPA 3-hourly precipitation rates for the TRMM period (1998–2013) (Yan et al., 2020). The hydrological outputs include routed runoff and discharges with spatial resolution of $0.125° \times 0.125°$ and time resolution of 3 hr. A grid cell is determined to be flooding when the routed runoff is greater than the predefined flood threshold. Specifically, a flood event is determined at a grid cell if there are at least four time steps with $R > P95 + 0.5 * \delta$ and $Q > 10$, where R is the routed runoff (mm); P95 and δ are the 95th percentile and temporal standard deviation of the routed runoff, respectively; and Q is the corresponding discharge (m^3/s). The combination of 95th percentile and δ provides better performance in flood event detection than percentile-only (e.g., 95th, 98th) and probabilistic approaches (e.g., Log Pearson type-III distribution) according to Wu et al. (2012), while the criteria $Q > 10$ can effectively reduce the false alarm rate particularly in dry areas (Wu et al., 2014). A time window of 24 time steps (i.e., 3 days corresponding to the 3-hr temporal resolution) is used to separate different flood events, similar as in Ward et al. (2016). The four monthly flood indices are then estimated at grid cells

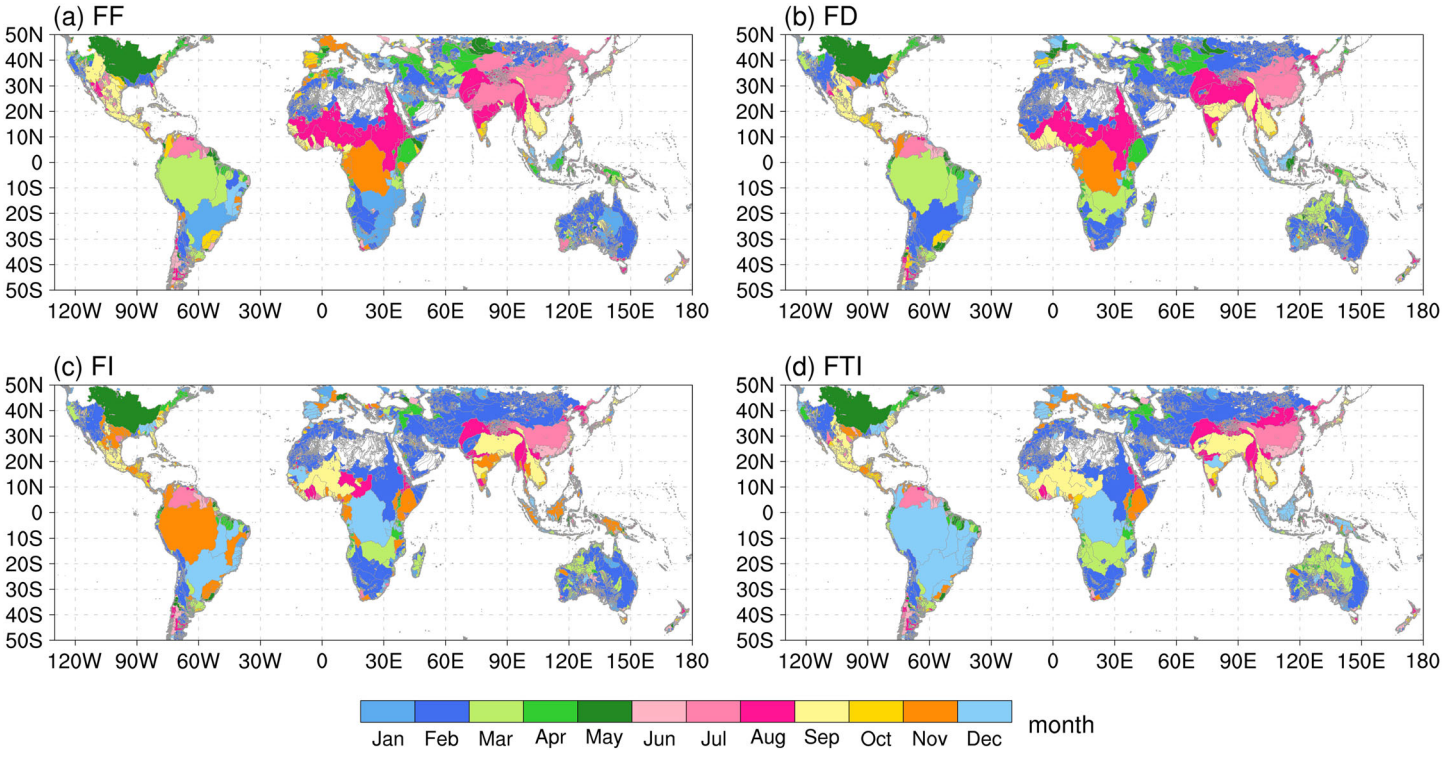

Figure 1. Peak months of flood indices for individual basins between 50°N and 50°S during 1998–2013. (a) Flood frequency (FF), (b) flood duration (FD), (c) flood intensity (FI), and (d) flood total intensity (FTI).

(Table S2), namely, flood frequency (FF), duration (FD), mean intensity (FI), and total intensity (FTI). Finally, monthly time series of these four indices averaged over every individual river basin between 50°N and 50°S are computed to represent basin-scale flood events and associated characteristics.

A series of monthly precipitation indices representing various aspects of daily precipitation characteristics are derived from the daily TRMM/TMPA precipitation product at the DRIVE model grids (Table S3), similar as in Yan et al. (2020). The basin-averaged precipitation indices are then computed and applied to represent basin-mean states of precipitation events. The ENSO events are represented by Niño 3.4, an index denoting sea surface temperature anomalies and variations within a domain of 5°N–5°S, 120°–170°W in the equatorial Pacific (http://www.cpc.ncep.noaa.gov/data/indices/).

3. Results and Discussion

3.1. Peak Flood Months

The peak flood months are identified first and compared with each other corresponding to four basin-mean flood indices (Figure 1). Successfully identifying the peak months for all individual river basins itself can result in an important account of global floods, which is very useful for further exploration of variations/changes in floods. For comparison, the peak months for basin-scale precipitation indices are determined as well (see Figure S1).

The peak months for FF are depicted in Figure 1a, clearly showing the annual preferred occurrence time of flood for each river basin. It is noted that certain coherent spatial structures connecting neighboring river basins with same peak flood months can readily be found across the world. For instance, August is the peak month for several individual river basins covering a large domain in equatorial central-west Africa. The peak flood months derived from FF tend to be consistent with the peak precipitation months for most river basins with good one-to-one correspondence (Figure S1). Nevertheless, over some regions such as in central South America and part of southeastern Asia, the peak precipitation months tend to be 1 month earlier than the peak flood months. For instance, in central South America, March is the peak month for those river basins,

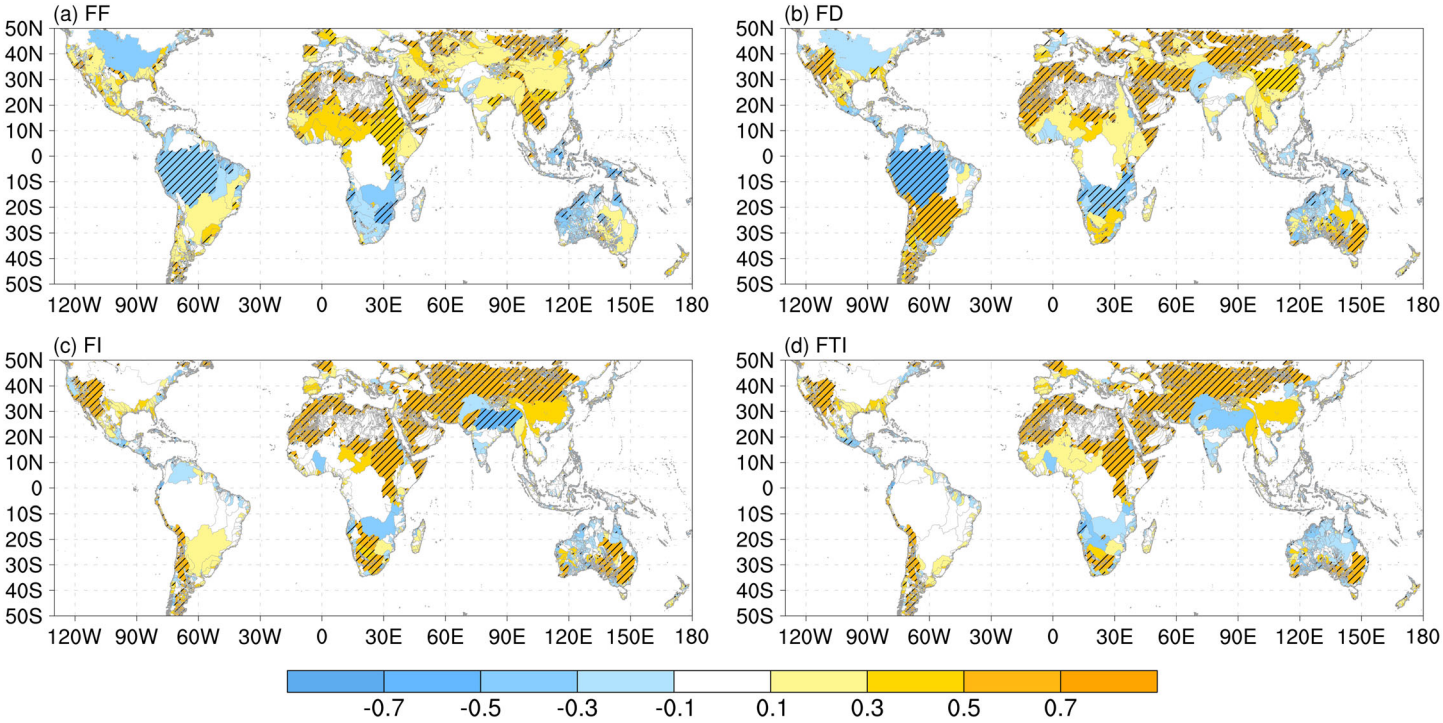

Figure 2. Simultaneous correlations between flood indices and Niño 3.4 in the respective peak months of four individual flood indices, i.e., (a) FF, (b) FD, (c) FI and (d) FTI. Striped lines denote those above the 90% confidence level.

while February is the peak month for precipitation indices except F01 and F10 whose peak month is March. This 1-month-lag between flood and precipitation may reflect the routing time particularly in large river basins and may also imply the indirect effect of preflood precipitation events through their modulation of antecedent surface conditions. The differences in peak months between flood and precipitation indices and between precipitation indices themselves might further suggest the existence of differing effects on floods of these precipitation indices representing various precipitation characteristics as discussed in Yan et al. (2020).

It is also of interest to note that over the same continent, the peak flood months could be different for different river basins (even for neighboring ones). These differences can also be found for precipitation indices, such as over northern South America and tropical East Africa. These basin-scale indices are used to represent the collective effect of an entire river basin/catchment with its reaches possibly with various distinct characteristics and perhaps even extending over different climate zones or regimes. However, the seemingly scattered spatial structure of peak months based on the basin-averaged indices roughly manifests the spatial distribution of hydroclimate regimes or seasonal variations of precipitation (e.g., Adler et al., 2017).

The peak months for FD are generally consistent with those for FF (Figures 1a and 1b). For FI and FTI, the peak months are approximately the same as each other for most basins (Figures 1c and 1d), while they tend to be different from those for FF and FD in many basins. These discrepancies imply that the most frequent flood month for a river basin might not necessarily be the month with those (most) intense flood events, at least gauged by basin-scale FI and FTI. For instance, more flood events tend to occur in the southern United States in February and March when FF reaches the peak, while the FI and FTI peaks tend to be found in November or December.

3.2. Simultaneous Correlations Between Floods and ENSO

Simultaneous correlations between the four flood indices and Niño 3.4 are estimated for their respective flood months (Figure 2). Here the 90% confidence level is used for both simultaneous and lag correlations, which is estimated based on the effective degrees of freedom (DOF) derived from the lag-one autocorrelations of the time series being correlated. For FF (Figure 2a), significant negative or positive correlations

appear in many river basins such as the Amazon River over South America, several river basins including the Nile river over the central-northern African continent, river basins scattered across northern Eurasia, and the Mekong and Pearl river basins in southeastern Asia. Similar spatial features can be seen for the correlations between FD and Niño 3.4 (Figure 2b), specifically with regard to the signs of correlation coefficients, indicating the similar effect of ENSO on FF and FD. FD shows stronger correlations than FF with ENSO in many river basins with only a few exceptions, such as over southeastern Asia, which is generally in agreement with Ward et al. (2016).

For comparison, simultaneous correlations between various basin-scale precipitation indices and Niño 3.4 are computed as well in the respective peak months for flood frequency index (FF; Figure S2) and for flood duration (FD; Figure S3). Spatial features of correlations with ENSO appear to be similar, with regard to the signs of correlation coefficients, between FF/FD and precipitation indices in many river basins (Figures 2a, 2(b), S2, and S3), even though obvious differences exist for other basins. In particular, significant correlations between either FF or FD and Niño 3.4 over North and South America, northern Eurasia, southern part of Africa, and Australia can also be found in Pr, F01, F10, and Pr01. This suggests that the ENSO effect on floods in these regions might mostly go through the ENSO-related variations in precipitation characteristics. From Figures 2 and S5, it is also seen that such ENSO effects on floods become weaker or more complicated (with sign changes or lagged-time) in river basins such as the Yangtze, Yellow, Nile, and Congo, which are in Asia and Africa continents with more complex continental hydroclimate and geographic components, and the Ganges and other river basins in the Indian subcontinent where other ocean-climate systems like the Indian Ocean Dipole (IOD) mode also have significant effects on precipitation and floods. It is further interesting to note that higher correlations between ENSO and FF/FD than for the precipitation indices can be seen for many basins. For instance, significant correlations exist in FF and FD for river basins from northern Africa to northern Eurasia, while the correlations tend to be weak for precipitation indices. It is possible that the ENSO signals might be much more discernible in basin-scale streamflow than in precipitation, as the former are a better indicator of water-cycle variations for a whole river basin (e.g., Chiew & McMahon, 2002). This might also imply that other mechanisms for the occurrence of floods could play a significant role in addition to precipitation.

For FI and FTI, the spatial structures of their simultaneous correlations with ENSO are generally similar with each other (Figures 2c and 2d), but tend to be different from those for FF and FD in many river basins partly due to their different peak months. Significant positive correlations appear over central-northern Africa and river basins in the Eurasian continent north of about 30°N, roughly consistent with the correlations for FF and FD, although they tend to be stronger. Positive correlations can also be seen in the southwestern United States, South Africa, and southeastern Australia. However, significant correlations are not found over most of tropical lands between 20°N and 20°S, with an exception of central-eastern Africa, i.e., in the Nile river basin. This might suggest that flood intensity (FI and FTI) could be more effectively modulated by other mechanisms than by ENSO, which warrants further exploration.

The correlations between precipitation indices and Niño 3.4 during the respective peak months for flood intensity (FI) are also computed for comparison (Figure S4). Spatial distributions of the ENSO correlations with precipitation are generally similar to those for FI/FTI. FI/FTI tend to have a stronger correlation with ENSO than precipitation indices north of about 20°N.

Given the differences in the peak months between FF/FD and FI/FTI, their ENSO relations are further examined by comparing their simultaneous correlations with Niño 3.4 corresponding to the respective peak months for individual river basins defined by FF (Figure S5). In contrast to Figure 2, these four flood indices generally show similar spatial features regarding their correlations with Niño 3.4, with only a few exceptions such as in the Mekong River and the Nile River. In particular, in contrast to Figure 2, both FI and FTI show certain correlations with ENSO in the tropics, though the connections still tend to be weak.

3.3. Lagged Correlations of Floods With ENSO

The possible lagged responses of floods to ENSO for individual river basins are further explored by estimating the correlations between Niño 3.4 and flood indices in their peak months, with the former leading by 0 to 6 months. The ENSO-leading months with maximum correlations between Niño 3.4 and flood indices in their respective peak flood months are then identified and illustrated in Figure 3. For FF (Figure 3),

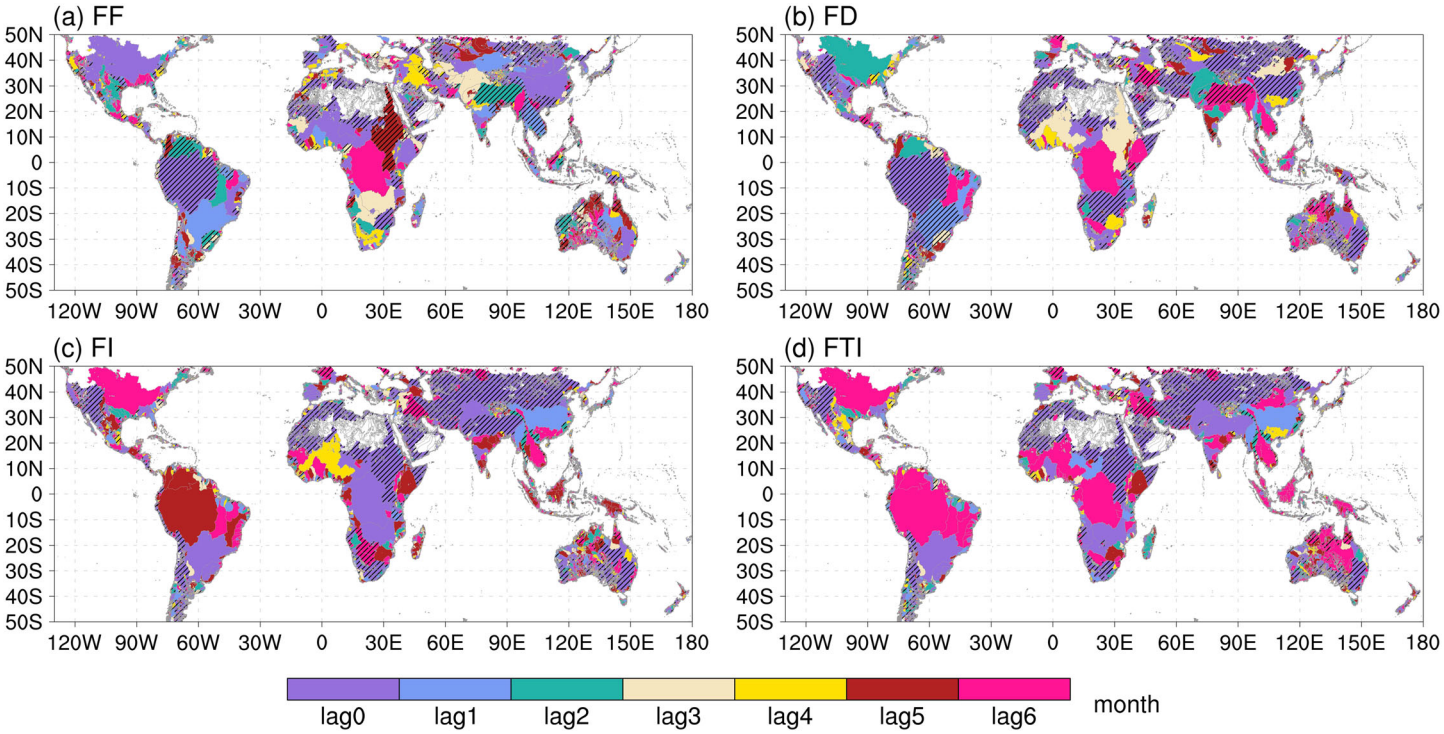

Figure 3. The Niño 3.4 leading months (including zero-lag month) with the highest correlations between Niño 3.4 and flood indices, i.e., (a) FF, (b) FD, (c) FI and (d) FTI, corresponding to their respective peak months. Striped lines denote those above the 90% confidence level.

maximum correlations with Niño 3.4 leading FF by 1 to 5 months appear in many river basins and can reach the 90% confidence level. For instance, significant correlation between Niño 3.4 and FF reaches its peak as the former leads by 1 month in the Mekong River; a 2-month ENSO-leading FF relation appears in the Orinoco River and Uruguay River over South America and there is a 5-month ENSO-leading FF relation for the Nile River. Furthermore, even though the simultaneous correlations with Niño 3.4 are the strongest for some other river basins including the Amazon River and the Pearl River, significant ENSO correlations can still be found as Niño 3.4 leads FF by several months (Figure 3a). These significant ENSO-leading-flood relations suggest the potential for monthly-to-seasonal flood forecast using ENSO as one of the essential predictors, which would benefit the preparedness for flood risk in these river basins.

For FD (Figure 3b), maximum correlations with Niño 3.4 leading FD can also be found in several river basins and are statistically significant at the 90% confidence level. The 1-, 3-, and 6-month ENSO-leading FD relations can be found for the Parana River, Uruguay River, and the Ganges river basin, respectively. For some other river basins with significant ENSO correlation, the simultaneous correlations are their maximum, including the Amazon River, the Zambezi River, the Yangtze River, the Murray-Darling basin, and river basins across northern Eurasia. Nevertheless, significant correlations between Niño 3.4 and FD can still be seen as the former leads by various months in these basins (Figure 3b), just as shown in Figure 3a for FF. Spatial similarities can generally be found between Figures 3a and 3b, 4a and 4b, though discrepancies appear in several regions. As mentioned above, the correlations between FD and Niño 3.4 tend to be stronger for many river basins, in addition to the differences in the ENSO-leading relations. However, when all the correlations are estimated corresponding to the peak months of FF, the discrepancies become relatively smaller (Figures S5 and S6), especially when we focus on the maximum ENSO-leading months (Figures S7a and S7b), though some differences still exist in East and southeastern Asia.

The lagged responses of precipitation indices to ENSO are also estimated for comparison for the peak months of FF (Figure S8). The ENSO responses corresponding to the peak months of FD are generally similar for every individual precipitation index (Figure S9). Comparing Figures 3b and S9, similar features can be found in certain basins, suggesting the role of precipitation in modulating floods by ENSO in those regions.

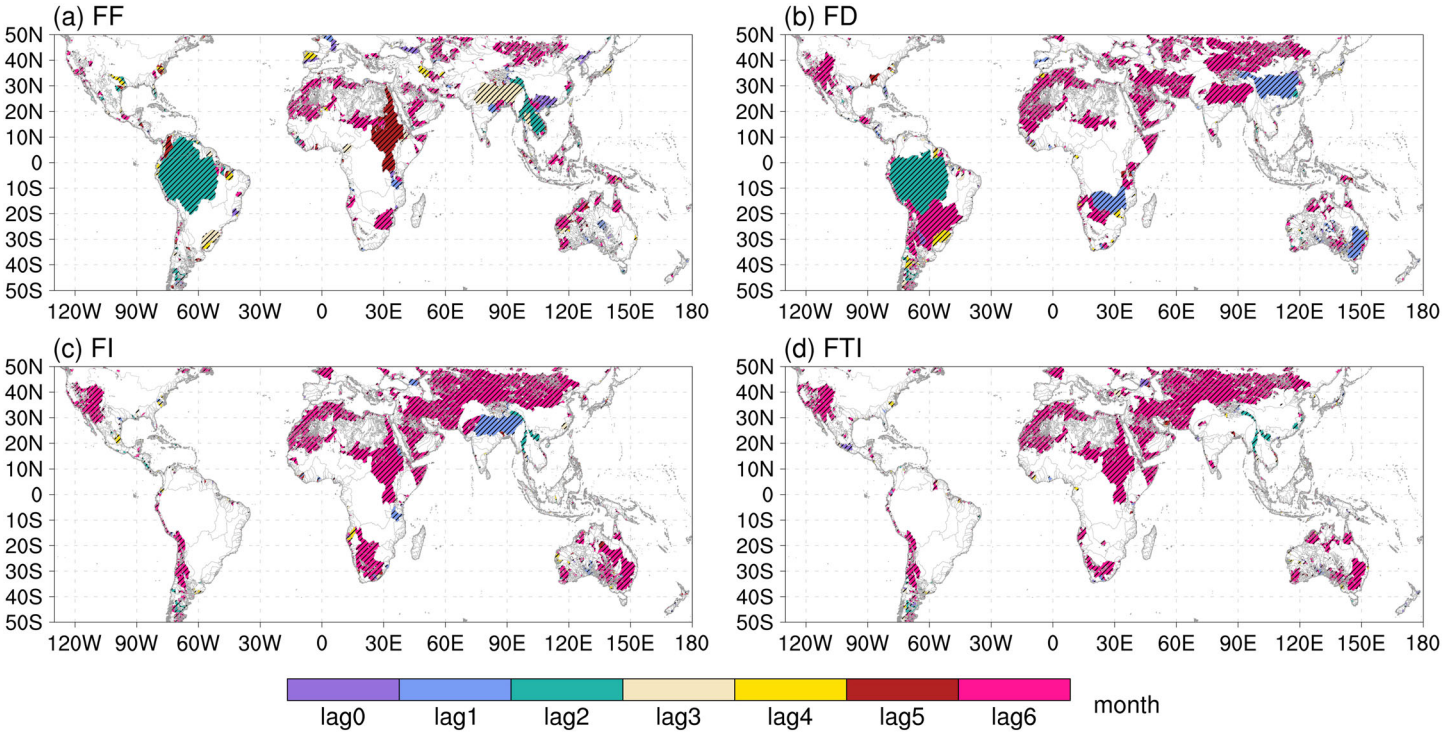

Figure 4. The maximum Niño3.4 leading months with the correlations between Niño 3.4 and flood indices (i.e., (a) FF, (b) FD, (c) FI and (d) FTI) which can reach the 90% confidence level corresponding to their respective peak flood months.

However, obvious discrepancies exist in many river basins with regard to the lag-relations with ENSO between FF/FD and precipitation indices. This suggests the existence of complex features relevant to the involvement of precipitation in the ENSO impact on floods for individual river basins (e.g., Emerton et al., 2017).

The ENSO-leading months with maximum correlations between Niño 3.4 and FI/FTI in their respective peak flood months are also estimated (Figures 3c–3d). General similarities can be found between Figures 3c and 3d, indicating the rough similar relations with ENSO between FI and FTI. Evident ENSO-leading relation can be observed in several river basins including the Okavango River in the southwest Africa and the Tigris-Euphrates in the Middle East. Significant correlations between Niño 3.4 and FI/FTI can appear as the former leads the latter by up to 6 months in many basins beyond the deep tropics (Figures 4c and 4d).

The lag-relations between FI/FTI and Niño 3.4 corresponding to the respective peak months defined by FF are also estimated for individual river basins (Figure S6). In contrast to Figure 3, these four flood indices generally manifest similar spatial features regarding their lagged responses to ENSO. In particular, there are several basins for which the lagged ENSO responses of either FI or FTI can be found, for instance, the Parana River, though similar significant relations do not exist for FF or FD. Similarities between FI/FTI and either FF or FD can further be seen when the maximum ENSO-leading months are all calculated corresponding to the peak months of FF except in the deep tropics, East and southeastern Asia, etc. (Figure S7).

4. Summary and Concluding Remarks

The ENSO impact on global floods during the TRMM period (1998–2013) is examined by using the streamflow outputs from the DRIVE model, which is driven by the high-spatiotemporal-resolution satellite-based precipitation product (TRMM/TMPA). Flood events for individual river basins between 50°N and 50°S are derived from the events at the DRIVE model grids estimated based on grid-based climatological thresholds of routed run-off, and their durations and magnitudes are determined accordingly. The peak flood months for river basins are then identified corresponding to the four flood indices: FF, FD, FI, and FTI. The

collective ENSO effects on each river basin during its peak flood month are then explored. In this study, we are primarily focused on the direct impact of ENSO on floods for individual river basins, though the ENSO effects on precipitation and associated daily precipitation characteristics are also examined for comparison.

Significant, simultaneous correlations between flood indices and Niño 3.4 appear in many flood-prone river basins in the tropics and across the midlatitudes of both hemispheres, including the Amazon River over South America, the Nile River over central-northern African continent, Murray-Darling basin in southeastern Australia, Mekong River in the southeastern Asia, Yangtze and Pearl river basins in China, rivers in southwestern United States, and river basins scattered across northern Eurasia. Significant ENSO-leading-floods relations gauged by significant lag-correlations between floods and Niño 3.4 can also be seen in many river basins across the world such as the Parana River, Orinoco River, and Uruguay River over South America; the Ganges river basin in south Asia; the Mekong River; and the Nile River. The ENSO impact on floods can sometimes be traced back to the modulation of various characteristics of precipitation events by ENSO for both simultaneous and leading/lagging relations, which confirms the ENSO-precipitation relations at the river basin scale. Nevertheless, the exact one-to-one correspondence between the ENSO effects on floods and precipitation cannot always be found for many basins, implying the likely involvements of other mechanisms in the occurrence of floods and associated variations.

The ENSO-floods-relations, especially the ENSO-leading-floods relations identified here for river basins/catchments of interest, can greatly enhance our understanding of how streamflow and then floods may vary on the interannual time scale and can further be applied to improve monthly-to-seasonal flood forecasting. The results can also provide useful guidance for flood preparedness, risk estimation, and management. However, this study is generally focused on the concurrent and lagged relations of river flows and floods with ENSO corresponding to the peak flood months. It is also likely that the ENSO effect on floods may vary with the diversity and temporal evolution of ENSO events (e.g., Emerton et al., 2017; Lee et al., 2018b). Therefore, more detailed mechanisms relevant to the ENSO effect on floods warrant further exploration. Furthermore, to fully understand how streamflow and floods vary on the larger-than-seasonal time scales and form an effective scheme for monthly-seasonal flood forecasts, the possible impacts from other physical modes such as the Pacific Decadal Oscillation (PDO), the North Atlantic Oscillation (NAO), and the Atlantic multidecadal oscillation (AMO) should be assessed and included as well (e.g., Emerton et al., 2017; Enfield et al., 2001; Lee et al., 2018b). Also, uncertainties may exist in both model simulations and satellite-based precipitation, which can limit the interpretation of the results. Thus, using other available precipitation products and models might be a feasible strategy in future research.

Data Availability Statement

All data used in this study are from Yan et al. (2020) and available online (http://flood.umd.edu/).

Acknowledgments

The authors thank the two anonymous reviewers for their constructive comments and suggestions. This study was supported by the National Key R&D Program of China (grant no. 2017YFA0604300) and National Natural Science Foundation of China (grants 41861144014, 41775106, and U1811464), and also partially by Natural Science Foundation of Guangdong Province (grant no. 2017A030313221) and the Program for Guangdong Introducing Innovative and Entrepreneurial Teams (no. 2017ZT07X355) and Guangdong Province Key Laboratory for Climate Change and Natural Disaster Studies (grant 2020B1212060025). PJW received additional funding from the Dutch Research Council (NWO) in the form of VIDI grant 016.161.324.

References

Adler, R. F., Gu, G., Sapiano, M., Wang, J. J., & Huffman, G. J. (2017). Global precipitation: Means, variations and trends during the satellite era (1979–2014). *Surveys in Geophysics*, *38*(4), 679–699. https://doi.org/10.1007/s10712-017-9416-4

Andrews, E. D., Antweiler, R. C., Neiman, P. J., & Ralph, F. M. (2004). Influence of ENSO on flood frequency along the California coast. *Journal of Climate*, *17*(2), 337–348. https://doi.org/10.1175/1520-0442(2004)017<0337:IOEOFF>2.0.CO;2

Archfield, S. A., Hirsch, R. M., Viglione, A., & Blöschl, G. (2016). Fragmented patterns of flood change across the United States. *Geophysical Research Letters*, *43*, 10,232–10,239. https://doi.org/10.1002/2016GL070590

Berghuijs, W. R., Woods, R. A., Hutton, C. J., & Sivapalan, M. (2016). Dominant flood generating mechanisms across the United States. *Geophysical Research Letters*, *43*, 4382–4390. https://doi.org/10.1002/2016GL068070

Chiew, F. H., & McMahon, T. A. (2002). Global ENSO-streamflow teleconnection, streamflow forecasting and interannual variability. *Hydrological Sciences Journal*, *47*(3), 505–522. https://doi.org/10.1080/02626660209492950

Curtis, S., & Adler, R. F. (2003). Evolution of El Niño-precipitation relationships from satellites and gauges. *Journal of Geophysical Research*, *108*(D4), 4153. https://doi.org/10.1029/2002JD002690

Dai, A., & Wigley, T. M. L. (2000). Global patterns of ENSO-induced precipitation. *Geophysical Research Letters*, *27*(9), 1283–1286. https://doi.org/10.1029/1999GL011140

Dettinger, M. D., & Diaz, H. F. (2000). Global characteristics of stream flow seasonality and variability. *Journal of Hydrometeorology*, *1*(4), 289–310. https://doi.org/10.1175/1525-7541(2000)001<0289:GCOSFS>2.0.CO;2

Emerton, R., Cloke, H. L., Stephens, E. M., Zsoter, E., Woolnough, S. J., & Pappenberger, F. (2017). Complex picture for likelihood of ENSO-driven flood hazard. *Nature Communications*, *8*(1), 1–9. https://doi.org/10.1038/ncomms14796

Emerton, R., Zsoter, E., Arnal, L., Cloke, H. L., Muraro, D., Prudhomme, C., et al. (2018). Developing a global operational seasonal hydro-meteorological forecasting system: GloFAS-Seasonal v1.0. *Geoscientific Model Development*, *11*(8), 3327–3346. https://doi.org/10.5194/gmd-11-3327-2018

Emerton, R. E., Stephens, E. M., & Cloke, H. L. (2019). What is the most useful approach for forecasting hydrological extremes during El Niño. *Environmental Research Communications*, *1*(3). https://doi.org/10.1088/2515-7620/1b114e

Enfield, D. B., Mestas-Nuñez, A. M., & Trimble, P. J. (2001). The Atlantic multidecadal oscillation and its relation to rainfall and river flows in the continental US. *Geophysical Research Letters*, *28*(10), 2077–2080. https://doi.org/10.1029/2000GL012745

Huffman, G. J., Bolvin, D. T., Nelkin, E. J., Wolff, D. B., Adler, R. F., Gu, G., & Hong, Y. (2007). The TRMM Multisatellite Precipitation Analysis (TMPA): Quasi-global, multiyear, combined- sensor precipitation estimates at fine scales. *Journal of Hydrometeorology*, *8*, 38–55. https://doi.org/10.1175/JHM560.1

Kumar, A., & Hoerling, M. P. (2003). The nature and causes for the delayed atmospheric response to El Niño. *Journal of Climate*, *16*(9), 1391–1403. https://doi.org/10.1175/1520-0442-16.9.1391

Lee, D., Ward, P., & Block, P. (2018a). Attribution of large-scale climate patterns to seasonal peak-flow and prospects for prediction globally. *Water Resources Research*, *54*(2), 916–938. https://doi.org/10.1002/2017WR021205

Lee, D., Ward, P. J., & Block, P. (2018b). Identification of symmetric and asymmetric responses in seasonal streamflow globally to ENSO phase. *Environmental Research Letters*, *13*(4). https://doi.org/10.1088/1748-9326/aab4ca/meta

Nobre, G. G., Muis, S., Veldkamp, T. I., & Ward, P. J. (2019). Achieving the reduction of disaster risk by better predicting impacts of El Niño and La Niña. *Progress in Disaster Science*, *2*, 100022. https://doi.org/10.1016/j.pdisas.2019.100022

Ropelewski, C. F., & Halpert, M. S. (1987). Global and regional scale precipitation patterns associated with the El Niño/Southern Oscillation. *Monthly Weather Review*, *115*(8), 1606–1626. https://doi.org/10.1175/1520-0493(1987)115<1606:GARSPP>2.0.CO;2

Sharma, A., Wasko, C., & Lettenmaier, D. P. (2018). If precipitation extremes are increasing, why aren't floods? *Water Resources Research*, *54*(11), 8545–8551. https://doi.org/10.1029/2018WR023749

Stephens, E., Day, J. J., Pappenberger, F., & Cloke, H. (2015). Precipitation and floodiness. *Geophysical Research Letters*, *42*, 10–316. https://doi.org/10.1002/2015GL066779

Trenberth, K. E., Branstator, G. W., Karoly, D., Kumar, A., Lau, N. C., & Ropelewski, C. (1998). Progress during TOGA in understanding and modeling global teleconnections associated with tropical sea surface temperatures. *Journal of Geophysical Research*, *103*(C7), 14,291–14,324. https://doi.org/10.1029/97jc01444

Ward, P. J., Beets, W., Bouwer, L. M., Aerts, J. C., & Renssen, H. (2010). Sensitivity of river discharge to ENSO. *Geophysical Research Letters*, *37*, L12402. https://doi.org/10.1029/2010GL043215

Ward, P. J., Eisner, S., Flörke, M., Dettinger, M. D., & Kummu, M. (2014). Annual flood sensitivities to El Niño–Southern Oscillation at the global scale. *Hydrology and Earth System Sciences*, *18*(1), 47–66. https://doi.org/10.5194/hess-18-47-2014

Ward, P. J., Jongman, B., Kummu, M., Dettinger, M. D., Weiland, F. C. S., & Winsemius, H. C. (2014). Strong influence of El Niño Southern Oscillation on flood risk around the world. *Proceedings of the National Academy of Sciences*, *111*(44), 15,659–15,664. https://doi.org/10.1073/pnas.1409822111

Ward, P. J., Kummu, M., & Lall, U. (2016). Flood frequencies and durations and their response to El Niño Southern Oscillation: Global analysis. *Journal of Hydrology*, *539*, 358–378. https://doi.org/10.1016/j.jhydrol.2016.05.045

Wu, H., Adler, R. F., Hong, Y., Tian, Y., & Policelli, F. (2012). Evaluation of global flood detection using satellite-based rainfall and a hydrologic model. *Journal of Hydrometeorology*, *13*(4), 1268–1284. https://doi.org/10.1175/JHM-D-11-087.1

Wu, H., Adler, R. F., Tian, Y., Huffman, G. J., Li, H., & Wang, J. (2014). Real-time global flood estimation using satellite-based precipitation and a coupled land surface and routing model. *Water Resources Research*, *50*, 2693–2717. https://doi.org/10.1002/2013WR014710

Wu, H., Li, X., Schumann, G. J.-P., Alfieri, L., Chen, Y., Xu, H., et al. (2020). From recent heavy precipitation in China to a glocal hydrometeorological solution for flood risk prediction. *Advances in Atmospheric Sciences*. https://doi.org/10.1007/s00376-020-0260-y

Yan, Y., Wu, H., Gu, G., Huang, Z., Alfieri, L., Li, X., et al. (2020). Climatology and interannual variability of floods during the TRMM era (1998–2013). *Journal of Climate*, *33*(8), 3289–3305. https://doi.org/10.1175/JCLI-D-19-0415.1